Continuous monitoring of cardiovascular function with a smart stent incorporating a flexible and stretchable wireless pressure sensor

IOP Publishing Journal of Micromechanics and Microengineering
J. Micromech. Microeng. **33** (2023) 115001 (9pp) https://doi.org/10.1088/1361-6439/acf7ce

Continuous monitoring of cardiovascular function with a smart stent incorporating a flexible and stretchable wireless pressure sensor

Nomin-Erdene Oyunbaatar[1,2], Arunkumar Shanmugasundaram[1,2], Kyeongha Kwon[3] and Dong-Weon Lee[1,2,4,*]

[1] MEMS and Nanotechnology Laboratory, School of Mechanical System Engineering, Chonnam National University, Gwangju 61186, Republic of Korea
[2] Medical Research Center for Cardiovascular Disease, Chonnam National University, Gwangju 61186, Republic of Korea
[3] School of Electrical Engineering, Korea Advanced Institude of Science and Technology, Daejeon 34141, Republic of Korea
[4] Center of Next-generation Sensor Research and Development, Chonnam National University, Gwangju 61186, Republic of Korea

E-mail: mems@jnu.ac.kr

Received 2 June 2023, revised 20 August 2023
Accepted for publication 8 September 2023
Published 15 September 2023

Abstract

The development of smart stents, capable of monitoring cardiovascular diseases and communicating vascular abnormalities to medical doctors, has garnered significant attention in the field of biomedical engineering. Various ex-situ fabrication strategies have been proposed to concurrently manufacture the smart stent and pressure sensor, thereby reducing the risk of sensor detachment caused by blood flow. However, the practical utility of these devices is still limited due to the rigidity of the wireless pressure sensor. In this study, we propose a flexible and stretchable smart self-reporting stent that incorporates a wireless pressure sensor. The fabrication process has been optimized to create a serpentine-shaped wireless pressure sensor that matches the shape and flexibility of the polymer stent struts. We thoroughly investigated the structural integrity, resonance frequency, stretchability, flexibility, and radial force of the manufactured smart self-reporting stent under different conditions. The wireless pressure sensor demonstrated a sensitivity of 0.15 MHz $mmHg^{-1}$, as determined through experimental analysis. To demonstrate the feasibility of the proposed smart stent, we implanted it into the arteries of a three-dimensional phantom system. The obtained results, combined with the flexible and stretchable nature of the proposed smart self-reporting stent, highlight its potential for effective monitoring of the heart's functional dynamics and detection of in-stent restenosis.

Keywords: ex-situ fabrication, smart self-reporting stent, flexible and stretchable stent, cardiovascular application

(Some figures may appear in colour only in the online journal)

* Author to whom any correspondence should be addressed.

1. Introduction

Cardiovascular diseases (CVD) remain a substantial global health concern, leading to a significant number of fatalities annually [1, 2]. Atherosclerosis, a prevalent form of CVD, involves the accumulation of plaque within blood vessels, resulting in arterial stiffening and an increased risk of myocardial infarction or stroke [3]. Stents are commonly used to alleviate arterial narrowing and restore blood flow, but the mechanical expansion of bare metal stents (BMS) often causes vascular trauma and subsequent neointimal hyperplasia, known as in-stent restenosis [4, 5]. Drug-eluting stents (DES) have been introduced to address the limitations of BMS and significantly reduce the incidence of in-stent restenosis [6]. However, as the drugs are gradually released from the stent's surface, the risk of vascular re-narrowing progressively increases. Bioabsorbable stents and bioabsorbable DES have been proposed as potential solutions to minimize adverse effects [7]. Despite significant advancements in stent technology, issues and complications such as in-stent restenosis, stent thrombosis, and re-narrowing of blood vessels may still arise after stent implantation or resorption of the polymer stent within the body [8–10]. For instance, thermoplastic polymer like poly lactic acid (PLA), polycaprolactone (PCL), polyglycolic acid (PGA) and poly-L-lactic acid (PLLA) emerging as suitable materials for crafting stents using 3D printing technology. They possess high flexibility, elasticity, and biodegradability, which can reduce the risk of long-term complications [11–13]. However, the development of polymer stents is still in progress, with the aim of expanding their applications in the biomedical field.

The integration of wireless pressure sensors into stents, known as smart stents, has garnered significant attention in the field of biomedical engineering [14–16]. These smart stents are designed to continuously monitor physiological parameters such as blood pressure and flow. By wirelessly transmitting biological information from the smart stent to an external readout device, healthcare professionals can gain comprehensive insights into the patient's cardiovascular system [17]. Over the years, various smart stent designs have been proposed for early detection of in-stent restenosis, utilizing different sensing principles including inductors, capacitors, transmitter microchips, and magnetoelastic sensors [18–23]. For instance, Takahata and Gianchandani were among the pioneers in suggesting the use of a smart stent equipped with a capacitive pressure sensor and an inductive stent antenna using micromachined silicon technology [24]. Subsequently, a biodegradable polymer stent incorporating a miniaturized MEMS-based capacitive pressure sensor was developed to detect a wide range of signals through electromagnetic wave transmission. Additionally, the integration of MEMS sensors into stainless steel stents was performed to enhance the stent's electromechanical performance *in vivo* [14–20]. A new chip made of pure steel with an embedded pressure sensor was created using laser micro-welding. However, the use of laser micro-welding and conductive adhesives may disrupt blood flow and increase the risk of sensor detachment from the stent due to blood flow, potentially leading to serious health issues and limiting the effectiveness of the smart stent. Despite advancements in integrating pressure sensors and stents, a methodology for the mass production of combined stents and pressure sensors has yet to be realized.

Recently, *in-situ* fabrication strategies have been proposed to enable the simultaneous fabrication of smart stents integrated with wireless pressure sensors. These fabrication techniques employ microelectromechanical systems (MEMS) and modified photolithography techniques to create a unified unit comprising the smart stent and pressure sensor. The utilization of ex-situ fabrication strategies offers several advantages over traditional methods of integrating pressure sensors into smart stents. By fabricating the pressure sensor and stent structure simultaneously, the number of fabrication steps needed for integrating the pressure sensor is reduced. This reduction in steps minimizes the risk of errors and enhances the accuracy of information provided by the smart stent. Furthermore, *in-situ* fabrication mitigates the potential problem of sensor detachment from the stent surface. For example, Kim *et al* proposed a wireless pressure sensor-integrated smart stent using a MEMS-based semiconductor process [25]. They achieved the self-rollable stent structure by controlling the radial stress of the material used. Similarly, Oyunbaatar *et al* proposed a self-rollable polymer stent integrated with a wireless pressure sensor for real-time monitoring of cardiovascular pressure. They employed thermo-compression bonding and residual stress to achieve the desired structure of the smart stent [26]. These stents, fabricated in a two-dimensional (2D) plane, exhibit superior structural integrity compared to conventional smart stent structures. This enhanced structural integrity reduces the risk of signal distortion caused by sensor packaging using conductive adhesives. However, the use of high temperatures during the self-assembling process of the 2D planar structure may result in an undesired rolling effect at the interface between the polymer stent strut and the wireless pressure sensor. This rolling effect occurs due to the rigidity of the wireless pressure sensor, which can deform differently compared to the more flexible polymer stent strut when subjected to high temperatures. Such a rolling effect can negatively impact the accuracy and reliability of the wireless pressure sensor, leading to incorrect readings and reducing the effectiveness of the smart stent in detecting in-stent restenosis.

In this study, we propose the demonstration of a smart self-reporting stent that integrates a flexible and stretchable wireless pressure sensor. To overcome the limitations of current state-of-the-art techniques, we optimized our fabrication strategies to create a serpentine-shaped wireless pressure sensor that matches the shape and flexibility of the polymer stent strut. This design approach allows the wireless pressure sensor and polymer stent strut to be flexible and stretchable while maintaining their functionality. This aspect is crucial for ensuring easy adaptation of the device within the blood vessels without causing damage or disrupting blood flow. We demonstrated the practical applicability of the proposed smart self-reporting stent by implanting it into the arteries of a 3D phantom, which accurately mimicked a real human heart system.

2. Materials and methods

2.1. Device concept and working mechanism

Figure 1 illustrates the proposed device concept and working mechanism of the smart self-reporting stent. The device is meticulously designed, taking into account the fabrication and assembly processes, material selection, and dimensional considerations to optimize performance, and flexibility. The wireless pressure sensor design incorporates a sandwich structure with flexible, serpentine-shaped top and bottom layers (figure 1(a)). The top layer consists of a capacitor plate and an inductor coil, while the bottom layer includes capacitor plates and an electrical connector. These layers are fabricated separately and then assembled using a thermal bonding process to form the wireless pressure sensor. To prevent direct contact between the top and bottom electrode layers, a thin layer of SU-8 (Kayaku Advanced Material, USA) photoresist is used to encapsulate the entire sensor. Figure 1(b) provides a schematic representation of the internal structure of the capacitive pressure sensor connected with the serpentine-shaped coil. The cross-sectional view clearly reveals the sandwiched configuration of the top and bottom layers, the presence of capacitor plates, the cavity area, and the serpentine-shaped inductor coil. The inductor coil, made of copper (Cu), is electro-patterned onto the serpentine-shaped polymer stent strut. The dimensions of the Cu inductor coil are carefully specified, with a width of 20 μm and inner and outer turn lengths of 10 and 43.2 mm, respectively. These dimensions ensure improved flexibility while maintaining the coil's structural integrity and functional effectiveness within the overall device. Figure 1(c) shows a schematic of the rolled 3D tubular-shaped smart stent integrated with the serpentine-shaped *LC* pressure sensor. The flexible diaphragm is placed at the middle of the inductor embedded with polymer stent, allowing for continuous monitoring of pressure changes.

The operating mechanism of the proposed wireless and batteryless pressure sensor is as follows. The capacitive element of the wireless pressure sensor consists of two capacitor plates separated by a 10 mm gap. The change in capacitance occurs as the gap between the capacitor plates undergoes a linear deformation in response to applied pressure. A change in capacitance causes a change in the resonance frequency of the *LC* circuit, and the change in blood vessel pressure is measured by precisely monitoring the frequency change as shown in figure 1(d) In addition, the external antenna circuit wirelessly detects and quantifies the resonance frequency changes, providing a direct indication of the varying pressure levels applied to the sensor. This innovative self-powered design of the sensor offers advantages for a wide range of applications, including wireless and energy-efficient sensing devices. The resonance frequency of the ideal sensor based on the LC circuit can be described mathematically as follows:

$$f_{\mathrm{r}} = \frac{1}{2\pi\sqrt{LC}} \tag{1}$$

where f_{r} is the resonance frequency of the *LC* circuit, L is the inductance of the coil, and C is the capacitance of the capacitor.

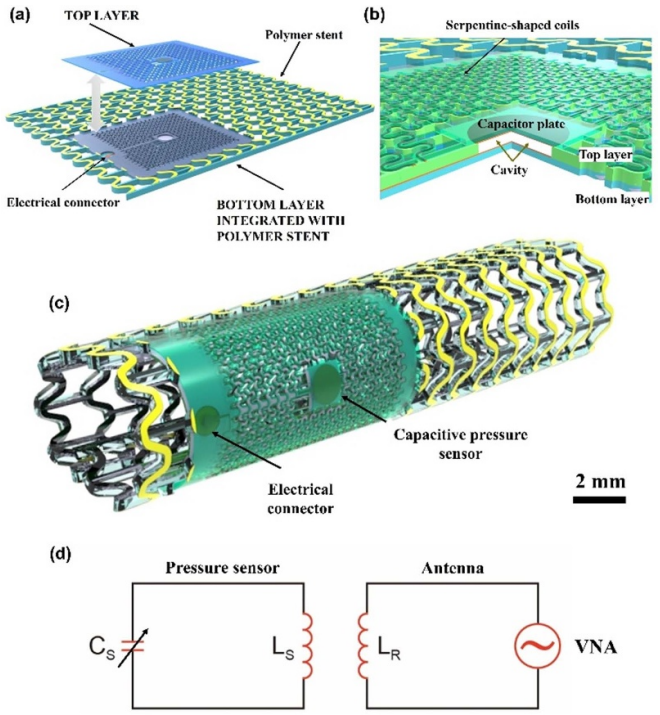

Figure 1. Schematic representation of (a) the device concept of the assembling top and bottom layers, (b) side view of the capacitor cavity after assembled top and bottom layers, and (c) self-rolled smart stent combined with a serpentine shaped wireless pressure sensor, (d) schematic of *LC* circuit.

2.2. Fabrication of smart self-reporting stent

To fabricate the smart stent using MEMS technology, an epoxy-based photosensitive polymer was employed as the base layer for both the stent itself and the *LC*-type capacitive pressure sensor. This choice was influenced by the biocompatibility and cytotoxicity attributes of the SU-8 polymer, as established in prior research [27, 28]. In the current study, we worked with two distinct SU-8 polymer series: SU-8 3000 and SU-2000. The fabrication process flow of the self-assembled, serpentine-shaped, smart self-reporting stent is schematically illustrated in figure 2. A 4-inch silicon wafer was used as the substrate for fabricating the polymer mesh structure, top capacitor plate, inductor coil, bottom capacitor plate, and electrical connector. Firstly, a 300 nm thick silicon dioxide (SiO_2) sacrificial layer was formed on the silicon wafer through wet oxidation (Lenton tube furnace, LFT, UK) at 1000 °C for 40 min. Subsequently, a 10 μm thick layer of SU-8 3010 was spin-coated onto the SiO_2 sacrificial layer at 2400 rpm for 40 s, providing a base for the sensor. Following this, a 10 nm thick titanium (Ti) layer and a 300 nm thick Cu metal seed layer were sputtered onto the SU-8 layer at 50 W for 1 h to fabricate the Cu inductor coil by oxidation furnace (ULTECH, SPT series, Korea). Next, the AZ P4620 photoresist (MicroChemicals, USA) was spin-coated onto the Ti/Cu layers at 1500 rpm for 30 s. The photoresist underwent a soft bake at 110 °C for 80 s, followed by UV curing at 9.5 mJ cm^{-2} for 90 s. The photoresist was then developed for 2 min using an AZ 340 developer (MicroChemicals, USA).

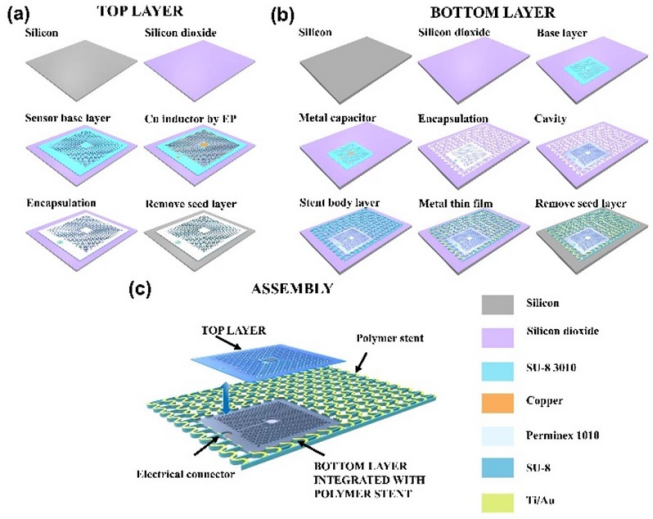

Figure 2. Schematic representation of the fabrication process flow for the proposed smart self-reporting stent. (a) Illustration of the fabrication of the top capacitor plate and electrical connector integrated with the polymer mesh structure. (b) Illustration of the fabrication of the bottom capacitor plate. (c) Illustration of the fabrication process flow for realizing the self-assembled serpentine-shaped smart self-reporting stent. The thermal bonding process is employed to assemble the top and bottom layers, transforming the polymer mesh structure into the self-assembled serpentine-shaped smart self-reporting stent configuration.

Subsequently, a 10 μm thick Cu layer was electrodeposited onto the SU-8 stent mesh structure, following the same pattern as the thick AZ4620, which served as an inductive layer. Then, 20 μm thick SU-8 negative photoresist was spin-coated on the inductor layer for serving body layer. Ultimately, the top capacitor plate with an inductor coil was released from the silicon wafer by dissolving the SiO_2 sacrificial layer with a buffered hydrofluoric acid (BHF, MicroChemicals, USA) solution, as illustrated in figure 2(a).

The fabrication procedure of the bottom capacitor plate is schematically illustrated in figure 2(b). In a typical fabrication process, a 300 nm thick SiO_2 sacrificial layer was formed on the silicon wafer following the methodology described in the previous section. Subsequently, SU-8 3010 was spin-coated onto the SiO_2 sacrificial layer at 2400 rpm for 40 s. Next, a 10 nm thick Ti layer and 100 nm thick Cu layer were sputtered onto the SU-8 3010 layer at 50 W for 1 h, enabling the fabrication of bottom capacitor plate. A capacitor plate with a diameter of 1 mm was patterned on the SU-8 layer utilizing a metal wet etching technique. Following, a 2 μm SU-8 was formed on the capacitor plate to serve as an insulating layer, preventing direct contact between the top and bottom layers. Consequently, 10 μm photosensitive Perminex layer (PermiNex® 1000, Kayaku Advanced Material, USA) was spin-coated on the insulating layer at 3000 rpm which was selectively opened only the capacitor area to facilitate the creation of an air cavity between the top and bottom capacitor plates. The Perminex layer not only functioned to form the capping cavity but also served as an adhesive for bonding the top and bottom layers due to its specific properties as an epoxy-based and photo-imageable. The optimized bonding parameters were set at 150 °C for 1 min, in accordance with the specifications provided in the Perminex 1000 series data sheet. Finally, the stent body layer was formed, and a metal thin layer was deposited on the stent body. The sacrificial SiO_2 layer was then removed from the silicon substrate using a BHF solution.

The alignment of the top capacitor with an inductor coil and electrical connector, as well as the bottom capacitor plate, was achieved utilizing a modified mask aligner. The modified mask aligner comprised a cover for securing the top plate, a micro stage for precise positioning, and a magnification-controlled optical microscope for accurate observation and alignment. Following the alignment process, the top and bottom capacitor plates were bonded together using a combination of thermal and hot-pressing techniques. This bonding was carried out at a temperature of 150 °C for 60 s, with an applied pressure of 850 gf cm^{-2}. The thermal and hot-pressing methods ensured a secure bond between the capacitor plates, which is crucial for the proper functioning of the self-assembled serpentine-shaped smart self-reporting stent (figure 2(c)). This bonding process not only provides structural integrity to the stent but also aids in maintaining the desired air cavity distance between the top and bottom capacitor plates, which is essential for reliable pressure sensing monitoring.

3. Result and discussion

The structural integrity and reliability of the proposed serpentine-shaped wireless pressure sensor integrated into the polymer stent mesh structure were thoroughly evaluated using an optical microscope, as shown in figure 3. Optical images of the top layer reveal the top capacitor plate and electrical connector combined with the serpentine-shaped polymer mesh structure (figure 3(a)). Similarly, optical images of the bottom layer exhibit the bottom capacitor plate, inductor coil, and electrical connector, all cohesively integrated with the serpentine-shaped polymer mesh structure (figures 3(b) and (c)). To assemble top and bottom layers, a thermal pressing process was utilized with 250 °C for 1 min. The 2D stent structure consisted of two capacitor plates positioned at its center and an inductor coil and electrical connector. A photograph showcases the fabricated serpentine-shaped wireless pressure sensor integrated into the polymer stent mesh structure after assembling the top and bottom capacitor plates, but before releasing it from the silicon substrate. The comprehensive analysis of the optical images of the top and bottom capacitor plates, as well as the examination of the assembled layers, demonstrates the successful integration of the various components. Moreover, it highlights the overall structural integrity of the serpentine-shaped wireless pressure sensor embedded within the polymer stent mesh structure.

The temperature-induced self-assembly process was employed to transform the two-dimensional (2D) serpentine-shaped wireless pressure sensor integrated polymer stent mesh structure into a three-dimensional (3D) smart self-reporting stent. To facilitate the self-assembly and control the curvature

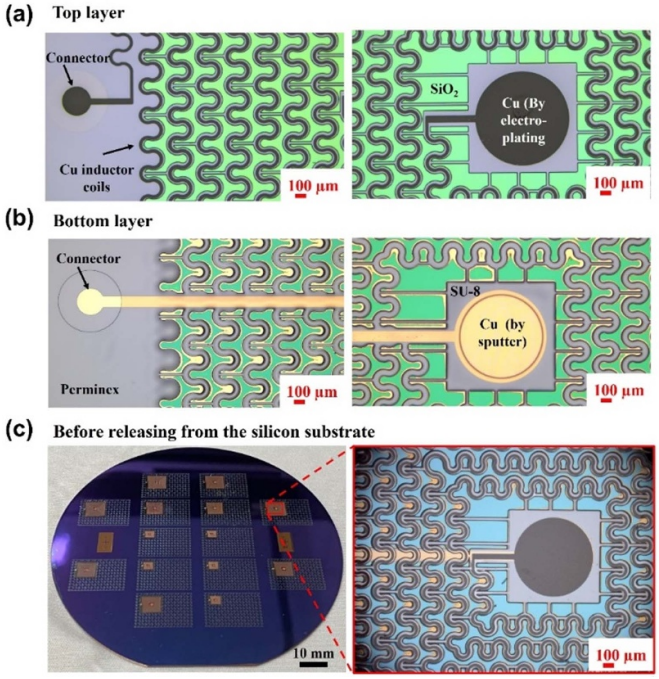

Figure 3. Assessment of the structural integrity of the proposed serpentine-shaped wireless pressure sensor integrated into the polymer stent mesh structure. (a), (b) Optical images illustrating the top capacitor plate and electrical connector in conjunction with the serpentine-shaped polymer mesh structure. (b) Optical images depicting the bottom capacitor plate, inductor coil, and electrical connector integrated with the serpentine-shaped polymer mesh structure. (c) Photograph shows the fabricated serpentine-shaped wireless pressure sensor integrated polymer stent mesh structure after assembling the top and bottom capacitor plates, but prior to release from the silicon substrate.

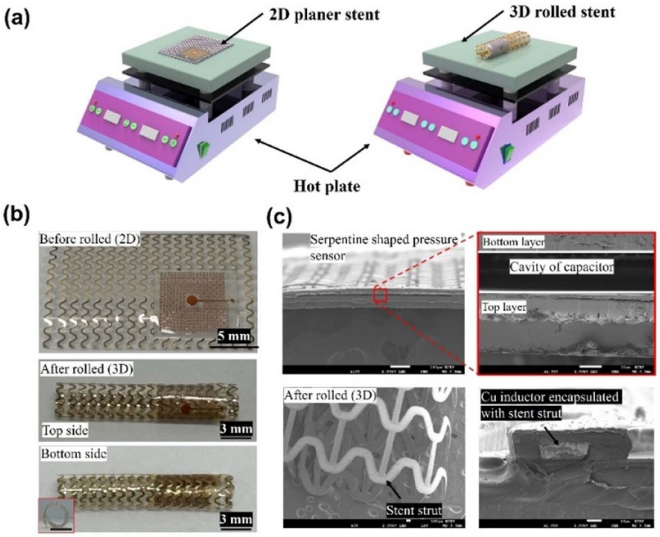

Figure 4. Fabrication of the smart self-reporting stent and evaluation of its structural integrity. (a) Schematic representation of the thermal technique employed to self-assemble the two-dimensional (2D) serpentine-shaped wireless pressure sensor integrated polymer stent mesh structure into a three-dimensional (3D) smart self-reporting stent. (b) Optical images displaying the fabricated serpentine-shaped wireless pressure sensor integrated polymer stent mesh structure after assembling the top and bottom capacitor plates, both before and after the self-assembly process. (c) Field emission scanning electron micrographs showcasing the fabricated serpentine-shaped wireless pressure sensor integrated polymer stent mesh structure after assembling the top and bottom capacitor plates, both prior to and following the self-assembly process.

during the transformation from a 2D mesh structure to a 3D stent structure, a 30 nm gold (Au) layer was fully patterned on the top layer of the polymer mesh structure. Subsequently, the structure was released using a BHF solution by dissolving the sacrificial oxide layer and detaching it from the silicon substrate. The dimensions of the stent mesh structure with the serpentine capacitive pressure sensor measured 12 × 18 mm in width and length, respectively. The 30 nm Au layer on the top surface of the stent mesh structure served as a catalyst for the self-assembly process. The disparity in chemical and physical properties between the Au and polymer mesh generated surface stress during high-temperature elevation. The fabricated 2D serpentine-shaped wireless pressure sensor integrated polymer stent mesh structure was placed on a pre-heated hot plate at 250 °C for 1 min. The Au layer exhibited a greater affinity for heat absorption compared to the underlying polymer mesh structure, leading to differential expansion and contraction rates, which consequently induced surface stress. This generated surface stress is facilitated by the temperature-induced self-assembly process allows for a controlled and precise transition between the 2D serpentine-shaped wireless pressure sensor integrated polymer stent mesh structure to self-assemble, ultimately forming the desired 3D stent structure as shown in figure 4(a).

Figure 4(b) shows the optical images of the fabricated serpentine-shaped wireless pressure sensor integrated polymer stent mesh structure, both before and after the self-assembly process. The optical images illustrate the successful integration of the various components and the overall structural integrity of the stent during self-assembly process. The field emission scanning electron micrographs (FE-SEM-JSM-7900F; JEOL) show a high-resolution perspective of the fabricated serpentine-shaped wireless pressure sensor integrated polymer stent mesh structure, both prior to and following the self-assembly process. The low magnification FE-SEM image demonstrates the formation of a uniform stent strut with consistent width and thickness in the smart self-reporting stent. Additionally, the high magnification image shows the Cu inductor coil encapsulated within the stent structure (figure 4(c)). The high-resolution FE-SEM images reveal the various components of the smart self-reporting stent, including the sandwich-structured top and bottom capacitor plates, as well as the capacitor cavity area (figure 4(d)). The top capacitor was designed as a thin layer to enable variations in capacitance, which in turn led to changes in the resonant frequency. This design approach ensures accurate and reliable measurements of pressure variations, ultimately contributing to the development of a highly functional and effective smart self-reporting stent for various medical applications.

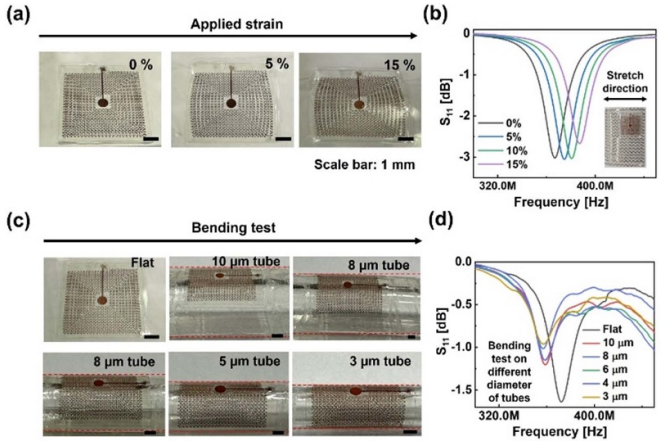

Figure 5. Mechanical stretchability and bending test of smart self-reporting stent. (a) Optical images of the fabricated serpentine-shaped wireless pressure sensor integrated smart self-reporting stent before and after lateral stretch at 0%, 5%, and 15%. (b) Resonance frequency changes with the degree of applied strain. (c) Photograph of the bending test if the serpentine-shaped wireless pressure sensor integrated smart self-reporting stent before (2D) and after bending on different degree of angles. (d) Resonance frequency of the serpentine-shaped wireless pressure sensor integrated smart self-reporting stent according to different applied bending angles.

Before commencing preliminary investigations, a stretching test was conducted to assess the sensitivity of the serpentine-shaped stretchable wireless pressure sensor in response to changes in applied strain. This comprehensive assessment aimed to explore the functionality of the smart self-reporting stent and its potential practical feasibility in biomedical application. The stretchable wireless pressure sensor was securely fastened at one end while the other end was connected to a motorized stretching apparatus. This apparatus provided precise control over the applied strain and facilitated measurements (figure 5(a)). During the stretching test, various levels of strain were applied to the sensor to simulate changes in the output signals. The resonance frequency of the stent was 367 MHz before any lateral stretching, and increased to 377, 381, and 387 MHz after lateral stretching at 5%, 10%, and 15% μm, respectively (figure 5(b)). The reason for the change of resonance frequency was inductive coupling between the two coils—antenna and a receiving coil in the wireless sensor. Lateral change of the inductor alters the current which powered through the magnetic field from the external antenna. Consequently, a bending test was performed with different bending angles. In figure 5(c) shows photograph of the serpentine shaped wireless pressure sensor attached on the different diameters of tube. As shown in figure 5(d) the resonance frequency was decreased from 370 MHz to 358 MHz when the serpentine-shaped wireless pressure sensor integrated smart self-reporting stent was attached to the tube with 10 μm in diameter (bending angle $\sim$15°). The resonance frequency was not changed further, increasing the bending angles only changed amplitude S_{11} parameter. It is causing the concentration of the magnetic field around the inductor.

The resonance frequency of the smart self-reporting stent was evaluated before and after the self-assembly process. An external antenna was positioned outside the pressure chamber and arranged perpendicularly above the smart stent. To analyze the resonant frequency of the smart stent, a network analyzer (model no. N9913B; KEYSIGHT) was employed. The resonance frequency of the serpentine-shaped wireless pressure sensor integrated smart self-reporting stent, both pre- and post-self-assembly process was found to be 368 and 354 MHz, respectively (figure 6(a)). The wireless pressure sensor was significantly smaller in size compared to the polymer stent. As a result, when the smart stent was subjected to high temperatures and rolled into its desired shape, there were no adverse effects on the reliability of the sensor or the effectiveness of the detection. The slight reduction in resonance frequency of the smart self-reporting stent after self-assembling was observed after transmission the smart stent from a 2D planar configuration to a 3D circular structure. These changes in the resonance frequency can be attributed to the alterations in inductance caused by the bending effect.

The radial force of the smart self-assembled is essential to evaluate its ability to withstand external pressure, maintain vessel patency, and prevent vessel recoil. Therefore, we evaluated the radial force of the fabricated smart self-reporting stent using a universal tensile machine (EZ-L; Shimadzu) with a periodic load applied to the stent. The fabricated smart self-reporting stent is placed between two parallel plates, where one plate is fixed, and the other movable plate compresses the stent radially. The fabricated smart self-reporting stent was compressed at 1 mm min^{-1} up to 1.4 mm and withdraw the applied pressure to its initial state and measured the entered force as a function of the applied compression displacement. The radial force of the smart self-reporting stent was found to be 0.04 N mm^{-1} (figure 6(b)). Inset in figure 6(b) shows the optical images of the fabricated smart self-reporting stent. This low radial force refers to less outward pressure exerted by the smart stent on the blood vessels during the deployment. As compared to higher radial force, polymer stent with lower radial force associated with less vessel wall injury and enhanced flexibility and conformability to the natural curvature of the vessel. Even though there are many advantages of the stent with low radial force, the mechanical properties of the stent are crucial value for preventing sudden deployment during the stenting procedure in the blood vessels. The low radial force of the smart self-reporting stent can be optimized through future research efforts, which may include the incorporation of nanostructures or the addition of functional additives. By integrating these advanced materials and design strategies, the performance of the smart self-reporting stent could be optimized to better address clinical requirements.

The special detection level of the smart self-reporting stent according to the position of external antenna, reflected detectable reading distance was investigated. The external antenna was moved perpendicularly away from the smart self-reporting stent in the range of 1 mm to 11 mm with the ramp of 1 mm. The Cu inductive coil was interfaced with an external antenna to generate a magnetic field, facilitating

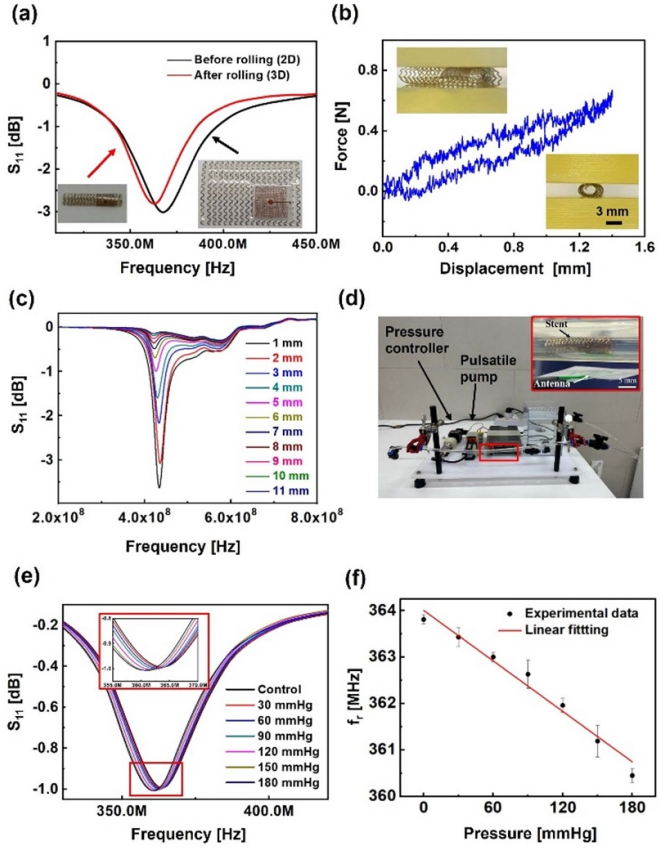

Figure 6. Preliminary characteristics of the smart self-reporting stent. (a) Resonance frequency of the serpentine-shaped wireless pressure sensor integrated with a smart self-reporting stent before (2D) and after self-assembling process. (b) Radial force of the serpentine-shaped wireless pressure sensor integrated smart self-reporting stent. Inset show the optical images of the fabricated smart self-reporting stents. (c) Resonance frequency of the serpentine-shaped wireless pressure sensor integrated with the smart self-reporting stent according to the external antenna reading distance. (d) Optical image of the experimental 3D phantom system setup. (e) Resonance frequency shift of the serpentine-shaped wireless pressure sensor integrated with the smart self-reporting stent according to different applied pressure. (f) Linear plot illustrating the relationship between applied pressure and the changes of resonance frequency.

the acquisition of the wireless pressure sensor signal from the smart self-assembled stent. A notable decrease in the amplitude of the stent's resonant frequency was observed as the distance between the external antenna and the stent increased from 1 mm to 11 mm. Despite the reduction in the amplitude of the resonant frequency with increasing antenna-to-stent distance, the smart self-assembled stent's resonant frequency remained detectable and measurable up to 11 mm (figure 6(c)). The resonance frequency of the fabricated smart self-reporting stent was investigated as a function of applied pressures ranging from 0 to 180 mmHg with ramp of 30 mmHg. The serpentine-shaped wireless pressure sensor integrated smart self-reporting stent was placed inside a pressure chamber (MMVC2S_S/4P, MS-TECH) for evaluating its resonance frequency. The inlet of the chamber was connected to a standard syringe pump, which was utilized to apply various pressure levels to the smart stent. Simultaneously, the other end of the pressure chamber was connected to a commercial pressure gauge, ensuring precise measurements of the applied pressure to the stent (figure 6(d)). The external antenna was positioned 5 mm away from the smart self-assembled during the measurements. The resonance frequency of the smart self-assembled stent was measured at each pressure level. The resonance frequency of the smart self-reporting stent decreased from 360 MHz to 354 MHz while applied pressure was increased from 0 to 180 mmHg. The enlarged region shows the change in resonance frequency of the smart stent when the applied pressure varied from 0 to 180 mmHg. The sensitivity of the proposed smart self-reporting stent was quantitatively assessed to ascertain the minimum detectable shift in resonance frequency that the device can distinguish. Through this evaluation, it was determined that the stent exhibits a sensitivity of 0.15 MHz $mmHg^{-1}$, indicating its capability to effectively detect subtle variations in pressure within the targeted physiological range (figure 6(e)). The linear relationship between the variation in resonance frequency and the sensitivity to applied pressure was clearly demonstrated in figure 6(f). The resonance frequency of the self-reporting stent was consistently decreased linearly with increasing applied pressure. The experiment result show that the sensitivity of the serpentine shaped wireless pressure sensor stable for passive detection of pressure changes.

The flexible capacitor's deflection response was precisely characterized using a high-precision laser vibrometer, ensuring accurate measurements and reliable data. The experimental setup involved incrementally applying pressure to the capacitor through a syringe pump, with pressure ranging from 0 to 300 mmHg. The corresponding deflection of the capacitor's membrane was meticulously recorded, resulting in a comprehensive understanding of its mechanical behavior under varying pressure conditions. As shown in figure 7(a), the membrane deflection displayed a notable response, reaching approximately 2.3 μm at a pressure of around 300 mmHg. Furthermore, figure 7(b) presents a detailed analysis of the capacitance changes concerning both the applied pressure and the deformation of the flexible capacitor. As the capacitor underwent deflection from 0 to 2.3 μm in response to varying applied pressure, the capacitance exhibited a gradual increase, ranging from 440 fF to 550 fF. These results highlight a strong correlation between the membrane deflection and the associated changes in capacitance, providing valuable insights into the functionality and performance of the flexible capacitor under different pressure conditions.

To evaluate the response time and sensitivity of the capacitive sensor, a tiny force was applied to the thin diaphragm of the capacitor and the resulting capacitance change was measured along with the corresponding response time. The experimental result is illustrated in figure 7(c). The laser vibrometer consistently maintained a signal noise level of approximately 200 nm (figures 7(d) and (e)) within the specified range, a testament to its remarkable precision in detection. Notably, the smallest deflection detected in the flexible membrane was 0.3 μm, showcasing the sensitivity of the capacitor to changes in applied pressure. This subtle displacement was

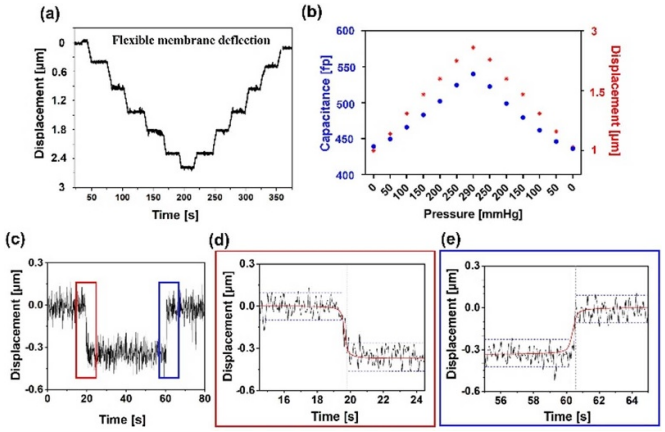

Figure 7. (a) The deflection of the flexible membrane in response to applied pressure as well as its recovery upon pressure release, which serves to assess the flexibility of the capacitor, (b) the corresponding changes in capacitance relative to the deflection of the flexible membrane, (c) the desplacement of the flexible membrane in response to applied pressure (20 mmHg), (d) and (e) the magnified section of the response time during the applied and released pressure, prespectively.

observed when subjecting the flexible capacitor to an applied pressure of approximately ∼20 mmHg, further affirming its responsiveness to subtle variations in pressure levels. The response recovery time during the application of 20 mmHg pressure to the flexible capacitor, facilitated through the syringe pump, was precisely determined to be 0.3 s. This rapid response time signifies the capacitor's ability to promptly adjust and stabilize its deflection in response to applied pressure changes.

4. Conclusion

In conclusion, the introduction of a flexible and stretchable wireless pressure sensor-integrated smart self-reporting stent is a significant advancement in biomedical engineering. The optimized fabrication strategies and thorough characterization of the device demonstrate its potential for monitoring the heart's functional dynamics and detecting in-stent restenosis. The smart self-reporting stent shows a strong linear relationship between changes in resonance frequency and sensitivity to applied pressure. It operates effectively in various environments, including *in vivo* conditions, as evidenced by comprehensive evaluations of its resonance frequency. Experimental integration into phantom arteries confirms its feasibility, allowing for the measurement of blood pressure and heart rate. The simplicity of the fabrication process, high sensitivity, and direct transfer of biological information make this smart self-reporting stent highly promising for practical applications in cardiovascular care.

Data availability statement

No new data were created or analysed in this study.

Acknowledgments

This study was supported by a National Research Foundation of Korea (NRF) Grant funded by the Korean Government (MSIT) (No. 2020R1A5A8018367).

ORCID iD

Dong-Weon Lee https://orcid.org/0000-0002-0847-4505

References

[1] Wilkins E, Wilson L, Wickramasinghe K, Bhatnagar P, Leal J, Luengo-Fernandez R R, Burns R, Rayner M and Townsend N 2017 *European Cardiovascular Disease Statistics* 2017 edn (European Heart Network)

[2] Cosselman K E, Navas-Acien A and Kaufman J D 2015 Environmental factors in cardiovascular disease *Nat. Rev. Cardiol.* **12** 627–42

[3] Im S H, Im D H, Park S J, Jung Y, Kim D H and Kim S H 2022 Current status and future direction of metallic and polymeric materials for advanced vascular stents *Prog. Mater. Sci.* **126** 100922

[4] Crimi G, Gritti V, Galiffa V A, Scotti V, Leonardi S, Ferrario M, De Ferrari G M, Oltrona Visconti L and Klersy C 2018 Drug eluting stents are superior to bare metal stents to reduce clinical outcome and stent-related complications in CKD patients, a systematic review, meta-analysis and network meta-analysis *J. Interv. Cardiol.* **31** 319–29

[5] Bønaa K H *et al* 2016 Drug-eluting or bare-metal stents for coronary artery disease *New Engl. J. Med.* **375** 1242–52

[6] Kuramitsu S, Sonoda S, Ando K, Otake H, Natsuaki M, Anai R, Honda Y, Kadota K, Kobayashi Y and Kimura T 2021 Drug-eluting stent thrombosis: current and future perspectives *Cardiovasc. Interv. Ther.* **36** 158–68

[7] Zablah J E, Morgan G J, Gropler M C, Shorofsky M and Prager J D 2022 Multidisciplinary approach to complex tracheobronchomalacia with a bioabsorbable stent *Prog. Pediatr. Cardiol.* **67** 101576

[8] Li H, Zhang W, Xia B, Sun F, Yang J and Zhang H 2021 Delayed coronary artery occlusion after transcatheter aortic valve replacement and chimney stenting: a case report *BMC Cardiovasc. Disord.* **21** 1–5

[9] Jan S, Gouëffic Y, Grimaud O and Le Meur N 2022 Hospitalization and death in the first 30 days after outpatient lower extremity arterial stenting *Cardiovasc. Interv. Radiol.* **45** 1441–50

[10] Haidegger M, Kneihsl M, Niederkorn K, Deutschmann H, Mangge H, Vetta C and Gattringer T 2021 Blood biomarkers of progressive atherosclerosis and restenosis after stenting of symptomatic intracranial artery stenosis *Sci. Rep.* **11** 15599

[11] Guerra A J, Cano P, Rabionet M, Puig T and Ciurana J 2018 3D-printed PCL/PLA composite stents: towards a new solution to cardiovascular problems *Materials* **11** 1679

[12] Chausse V, Iglesias C, Bou-Petit E, Ginebra M P and Pegueroles M 2023 Chemical vs thermal accelerated hydrolytic degradation of 3D-printed PLLA/PLCL bioresorbable stents: characterization and influence of sterilization *Polym. Test.* **117** 107817

[13] Sousa A M, Amaro A M and Piedade A P 2022 3D printing of polymeric bioresorbable stents: a strategy to improve both cellular compatibility and mechanical properties *Polymers* **14** 1099

[14] Chen X, Assadsangabi B, Hsiang Y and Takahata K 2018 Enabling angioplasty-ready "Smart" Stents to detect in-stent restenosis and occlusion *Adv. Sci.* **5** 1700560
[15] Park J, Kim J K, Patil S J, Park J K, Park S and Lee D W 2016 A wireless pressure sensor integrated with a biodegradable polymer stent for biomedical applications *Sensors* **16** 809
[16] Son D, Lee J, Lee D J, Ghaffari R, Yun S, Kim S J and Kim D H 2015 Bioresorbable electronic stent integrated with therapeutic nanoparticles for endovascular diseases *ACS Nano* **9** 5937–46
[17] Chow E Y, Chlebowski A L, Chakraborty S, Chappell W J and Irazoqui P P 2010 Fully wireless implantable cardiovascular pressure monitor integrated with a medical stent *IEEE Trans. Biomed. Eng.* **57** 1487–96
[18] Chen X, Brox D, Assadsangabi B, Ali M S M and Takahata K 2017 A stainless-steel-based implantable pressure sensor chip and its integration by microwelding *Sens. Actuators* A **257** 134–44
[19] Green S R, Kwon R S, Elta G H and Gianchandani Y B 2010 *In situ* and *ex vivo* evaluation of a wireless magnetoelastic biliary stent monitoring system *Biomed. Microdevices* **12** 477–84
[20] Park J, Kim J-K, Kim D-S, Shanmugasundaram A, Park S A, Kang S, Kim S-H, Jeong M H and Lee D-W 2019 Wireless pressure sensor integrated with a 3D printed polymer stent for smart health monitoring *Sens. Actuators* B **280** 201–9
[21] Takahata K, Gianchandani Y B and Wise K D 2006 Micromachined antenna stents and cuffs for monitoring intraluminal pressure and flow *J. Microelectromech. Syst.* **15** 1289–98
[22] Chow E Y, Beier B L, Francino A, Chappell W J and Irazoqui P P 2009 Toward an implantable wireless cardiac monitoring platform integrated with an FDA-approved cardiovascular stent *J. Interv. Cardiol.* **22** 479–87
[23] Herbert R, Lim H R, Rigo B and Yeo W H 2022 Fully implantable wireless batteryless vascular electronics with printed soft sensors for multiplex sensing of hemodynamics *Sci. Adv.* **8** eabm1175
[24] Takahata K and Gianchandani Y B 2004 A planar approach for manufacturing cardiac stents: design, fabrication, and mechanical evaluation *J. Microelectromech. Syst.* **13** 933–9
[25] Kim D S, Oyunbaatar N E, Shanmugasundaram A, Jeong Y J, Park J and Lee D W 2022 Stress induced self-rollable smart-stent-based U-health platform for in-stent restenosis monitoring *Analyst* **147** 4793–803
[26] Oyunbaatar N E, Kim D S, Prasad G, Jeong Y J and Lee D W 2022 Self-rollable polymer stent integrated with wireless pressure sensor for real-time monitoring of cardiovascular pressure *Sens. Actuators* A **346** 113869
[27] Nemani K V, Moodie K L, Brennick J B, Su A and Gimi B 2013 *In vitro* and *in vivo* evaluation of SU-8 biocompatibility *Mater Sci. Eng.* C **33** 4453–9
[28] Wang L, Wu Z Z, Xu B, Zhao Y and Kisaalita W S 2009 SU-8 microstructure for quasi-three-dimensional cell-based biosensing *Sens. Actuators* B **140** 349–55